Acta Biomaterialia 72 (2018) 396–406

Contents lists available at ScienceDirect

Acta Biomaterialia

journal homepage: www.elsevier.com/locate/actabiomat

Full length article

Porous calcium phosphate glass microspheres for orthobiologic applications

Kazi M. Zakir Hossain [a], Uresha Patel [a], Andrew R. Kennedy [a,1], Laura Macri-Pellizzeri [b], Virginie Sottile [b], David M. Grant [a], Brigitte E. Scammell [c], Ifty Ahmed [a,*]

[a] Advanced Materials Research Group, Faculty of Engineering, University of Nottingham, Nottingham NG7 2RD, UK
[b] Wolfson STEM Centre, Division of Cancer and Stem Cells, School of Medicine, University of Nottingham, Nottingham NG7 2UH, UK
[c] Faculty of Medicine & Health Sciences, Queen's Medical Centre, Nottingham NG7 2UH, UK

ARTICLE INFO

Article history:
Received 9 January 2018
Received in revised form 7 March 2018
Accepted 22 March 2018
Available online 29 March 2018

Keywords:
Calcium phosphate glass
Porous microspheres
Stem cells

ABSTRACT

Orthobiologics is a rapidly advancing field utilising cell-based therapies and biomaterials to enable the body to repair and regenerate musculoskeletal tissues. This paper reports on a cost-effective flame spheroidisation process for production of novel porous glass microspheres from calcium phosphate-based glasses to encapsulate and deliver stem cells. Careful selection of the glass and pore-forming agent, along with a manufacturing method with the required processing window enabled the production of porous glass microspheres via a single-stage manufacturing process. The morphological and physical characterisation revealed porous microspheres with tailored surface and interconnected porosity (up to 76 ± 5%) with average pore size of 55 ± 8 μm and surface areas ranging from 0.34 to 0.9 $m^2 g^{-1}$. Furthermore, simple alteration of the processing parameters produced microspheres with alternate unique morphologies, such as with solid cores and surface porosity only. The tuneable porosity enabled control over their surface area, degradation profiles and hence ion release rates. Furthermore, cytocompatibility of the microspheres was assessed using human mesenchymal stem cells via direct cell culture experiments and analysis confirmed that they had migrated to within the centre of the microspheres. The novel microspheres developed have huge potential for tissue engineering and regenerative medicine applications.

Statement of Significance

This manuscript highlights a simple cost-effective one-step process for manufacturing porous calcium phosphate-based glass microspheres with varying control over surface pores and fully interconnected porosity via a flame spheroidisation process. Moreover, a simple alteration of the processing parameters can produce microspheres which have a solid core with surface pores only. The tuneable porosity enabled control over their surface area, degradation profiles and hence ion release rates. The paper also shows that stem cells not only attach and proliferate but more importantly migrate to within the core of the porous microspheres, highlighting applications for bone tissue engineering and regenerative medicine.
Crown Copyright © 2018 Published by Elsevier Ltd on behalf of Acta Materialia Inc. All rights reserved.

1. Introduction

Orthobiologics is a rapidly advancing field which utilises cell-based therapies and biomaterials to promote healing. The development of orthobiologic solutions for repairing musculoskeletal disorders has become the main focus of orthopaedic procedures in recent years [1]. Orthobiologics have been utilised in a variety of different areas of medicine and their applications continue to expand which is enabling orthobiologics to emerge as the frontline for disease treatment and has the potential to revolutionise medicine [2].

The advantages of using synthetic biomaterials over autograft and allograft bone materials are associated with their ease of availability and significantly reduced the risk of infection from donor material as well as their scale-up manufacturing and long-term preservation in order to supply on-demand [3,4]. It was discovered

* Corresponding author.
E-mail address: Ifty.Ahmed@nottingham.ac.uk (I. Ahmed).
[1] Current address: Engineering Department, Lancaster University, Lancaster LA1 4YW, UK.

https://doi.org/10.1016/j.actbio.2018.03.040
1742-7061/Crown Copyright © 2018 Published by Elsevier Ltd on behalf of Acta Materialia Inc. All rights reserved.

that bioactive glasses could be used to stimulate osteogenesis, thereby leading to the concept of tissue regeneration. It has also since been discovered that the dissolution ion products from these glasses could also provide signals to the cells [5].

The three main types of bioactive glasses investigated for biomedical applications include silicates, borates and phosphate-based glasses. Silicate-based bioactive glasses are based on SiO_2 (as the glass network former) and include other modifying oxides such as Na_2O, CaO and P_2O_5 (and were initially developed by the late Professor Larry Hench and commercialised as 45S5 Bioglass™ [6]). They have to a great extent been applied for use in hard tissue repair [6–8] and more recently have been added to toothpaste (Sensodyne®, Novamin™, BioMin). Borate-based glasses (where B_2O_3 is the glass network former) degrade faster than silicate-based glasses and have also been investigated for biomedical applications [9]. Huang et al. [9] investigated the formulation B_2O_3 46.1 – CaO 26.9 – Na_2O 24.4 – P_2O_5 2.6 (in mol%) and found that they could convert this glass into apatite following immersion within a dilute (0.02 M) K_2HPO_4 solution. Phosphate-based glasses are based on P_2O_5 (as the glass network former) and have been widely explored using Na_2O and CaO including many other modifying oxides such as CuO [10], Ag_2O [11], TiO_2 [12], SrO [13], MgO [14] to provide enhanced properties or biological responses [15–19]. The main advantage of phosphate glasses over the silicate-based bioglasses and bioceramic materials include their fully degradable and controllable resorption profiles (which can range from days/weeks/to many months), by simply tailoring the glass formulations [20,21].

Microspheres (i.e. spherical particles) produced from polymers [22], bioactive glasses [23], and ceramics [24] exhibit greater advantages over irregular-shaped particles such as improved flow properties, which would be particularly beneficial for biomedical applications (for example, by enabling improved delivery via minimally invasive surgical injection procedures [25]). In addition, microspheres can be engineered to be porous or hollow which would provide a larger surface area allowing for encapsulation of other biomedically relevant components with an increase in degradation rate and beneficial ion release profile [22,26,27]. Microparticles with hollow and/or porous morphologies have become extremely important in many scientific fields due to their advantageous functional properties. For example, hollow microspheres have been exploited as additives for adhesives and as fillers in construction composites due to their durability and lightweight [28], whereas porous microparticles have been widely investigated for applications varying from stem cell research [29,30], drug delivery [31], tissue engineering [32], separation sciences [33], supercapacitors [34] and energy storage [35]. More recently, hollow glass microspheres with porous walls (with porosity on the angstrom level) have been developed and are being investigated to store liquids and gases within their hollow interior with the aim to release them on demand [27]. However, the development of highly porous glass microspheres via a simple manufacturing process, with controlled surface porosity levels and with interconnected porosity (throughout the entire microsphere), could have the potential to totally revolutionise the microsphere industry by enabling many other applications for these materials.

Manufacturing processes for porous materials depend heavily on the type of material used. For example, techniques utilised for making porous glass and/or ceramic scaffolds commonly use methods such as incorporation of a removable space holder [36], polymer foam replication [37], sol-gel [38], gel cast foaming [39] and solid freeform methods (i.e. 3D printing) [40]. These manufacturing processes involve multiple processing steps which can be laborious, time-consuming and energy intensive. The dissolution and thermal decomposition of space holders and sacrificial polymer templates can also result in residual contaminants which not only affects further processing but also the mechanical and physical properties of the resultant porous material. In the case of solid freeform fabrication techniques (3D printing), maintaining the viscosity of the ink (glass particles along with the polymer binder) is critical and can be time-consuming requiring several steps of printing, drying and sintering [40].

Processes utilised for manufacturing polymer based porous microspheres have mostly been via emulsion-solvent evaporation, spray drying and phase separation techniques [31,41,42]. Whilst, ceramic microspheres have commonly been fabricated via gelation, emulsification and precipitation processes [24,43] and solid (non-porous) and hollow glass microspheres have been fabricated via sol-gel [44] and flame spheroidisation [23] processes. However, when considering the manufacture of porous glass microspheres with fully controlled surface and interconnected porosity, the main challenges have included lengthy and/or complex manufacturing processes (for example, production costs associated with traditional phase-separated alkali borosilicate glasses, which are heat treated for 24 h and then further mineral acid leaching protocols applied [27,45]), scale-up limitations and control over pore size, interconnected porosity and morphology.

In this paper, the authors report a new and simple process for manufacturing highly porous calcium phosphate (CaP) glass microspheres with tailorable surface and fully interconnected porosity (up to 76%) within each microsphere produced, via a single-stage flame spheroidisation process. Preliminary biological analyses were performed via indirect and direct cell culture studies using human bone marrow-derived mesenchymal stem cells (hBM-MSCs) confirming the suitability of these microspheres to support cell adhesion and growth.

2. Materials and methods

2.1. Manufacture of solid and porous calcium phosphate glass microspheres

Calcium phosphate glass in the system $40P_2O_5{\cdot}16CaO{\cdot}24MgO{\cdot}20Na_2O$ (mol% denoted as P40) was prepared using NaH_2PO_4, $CaHPO_4$, $MgHPO_4$ and P_2O_5 (Sigma-Aldrich, UK) as starting materials, as described elsewhere [46,47]. These precursors were placed into a 100 ml volume Pt/5%Au crucible and dried at 350 °C for 30 min in a furnace. The sample was then melted at 1150 °C for 90 min. The molten glass was then quenched onto a steel plate and allowed to cool to room temperature.

Once cooled, the glass was ground into microparticles using a Retsch PM100 milling machine and sieved into varying size ranges spanning 63–300 μm. The solid non-porous microspheres were produced using the flame spheroidisation method which utilised an oxy/acetylene flame spray gun (MK 74, Metallisation Ltd, UK). Porous glass microspheres were produced by introducing various ratios of blended glass powder and calcium-based carbonate porogen (at ratios of 1:1, 1:2 and 1:3) into the flame of the thermal spray gun (using oxy-acetylene ratio of 3:3). Post-manufacture, the microspheres were collected from cooling trays and were then subjected to an acid wash step by gently stirring them in acetic acid (5 M) for 2 min followed by washing using deionised water (for 5 min) and then dried in an oven at 50 °C for 24 h.

2.2. Characterisation methods

2.2.1. Scanning electron microscopy (SEM) and energy dispersive X-ray (EDX) analysis

The surface and cross-sectional morphology were qualitatively examined using scanning electron microscopy (SEM – Philips XL30, FEI, USA) operated at 20 kV. Cross sections were achieved

by embedding the microspheres in a cold set epoxy resin and polished with SiC paper followed by a diamond cloth. Quantitative compositional analysis of the CaP microspheres was carried out using an energy dispersive X-ray (EDX, INCA Oxford Instruments) detector at an accelerating voltage of 20 kV and a working distance of 10 mm. All samples were carbon coated using an evaporation coater (Edwards coating System E306A) in order to avoid image distortion due to charging.

2.2.2. Mercury porosimetry and BET surface area analysis

The porosity of the microspheres was investigated using mercury intrusion porosimetry (Micromeritics Autopore IV 9500). A 5 cc powder penetrometer (Micrometrics) with 1 cc intrusion volume was used for all samples. An empty penetrometer test was also conducted as a blank before running the samples.

The surface area was determined via gas adsorption using the BET technique (Micrometrics Gemini 2360) where approximately 0.5 g of the microspheres were initially degassed under nitrogen at 110 °C for at least 2 h before performing multipoint BET analysis.

2.2.3. Degradation and ion release studies

Degradation analyses of the microspheres were evaluated by means of mass loss measurements in ultra-purified water (Milli-Q) (1% w/v) at 37 °C over 28 days (the medium was refreshed every 2 days). The degraded microspheres were removed from the medium at various time points (1, 3, 7, 14, 21, and 28 days) and placed onto tissue paper to blot dry then weighed immediately.

$$Mass\,Loss\,(\%) = \frac{M_0 - M_t}{M_0} \quad (1)$$

where M_o is the initial mass and M_t is the mass at test time point t.

Ion release profiles of the microspheres were conducted in low glucose Dulbecco's Modified Eagle Medium (DMEM, ThermoFisher Scientific, UK) (1% w/v) over 14 days (the media was again refreshed every 2 days) using inductively coupled plasma mass spectrometry (ICP-MS, Thermo-Fisher iCAP-Q model).

2.2.4. Cell culture study

2.2.4.1. Preparation of CaP microspheres extract. Porous CaP microspheres were sterilised through two 15 min wash steps using 70% EtOH [48,49]. After complete evaporation of 70% EtOH at room temperature in sterile conditions, porous microspheres were soaked in standard cell culture (SC) medium (low glucose DMEM (Gibco) supplemented with 10% foetal calf serum (ThermoFisher Scientific, UK), 1% penicillin and streptomycin, 1% L-Glutamine, 1% of non-essential amino acids) at a final concentration of 100 mg ml^{-1} at 37 °C and 5% CO_2. After 24 h, the conditioned medium containing the microsphere ion extracts was collected, filtered using 0.22 μm syringe filters and used to prepare three serial dilutions with 1:10 ratio using SC medium.

2.2.4.2. MTT assay. The evaluation of cytotoxicity was performed using a "Cell Growth Determination Kit, MTT based" (Sigma-Aldrich, UK) in accordance with ISO-10993-5:2009; for this purpose, 1×10^4 immortalised human bone marrow-derived mesenchymal stem cells (hBM-MSCs) [50–52] were seeded in 96-well plate in 100 μl of SC medium. After 24 h, SC medium was replaced with ion extract conditioned medium or the 3 serial dilutions prepared as shown in Section 2.2.4.1. Moreover, SC medium alone or supplemented with 5% of DMSO were included as controls. After 24 h, cells were washed once with PBS and incubated during 3 h at 37 °C and 5% of CO_2 with a SC medium supplemented with 10% of MTT solution. After incubation, media was aspirated and 100 μl of DMSO was added to each well and incubated for 15 min in gentle shaking to facilitate the formazan salts dissolution. Absorbance was read using a plate reader at 570 nm, setting 650 nm as reference. The cell viability percent was calculated in comparison to SC medium control using the following formula:

$$Viability(\%) = \frac{OD570s}{OD570c} \quad (2)$$

where, *OD*570s and *OD570c* are the optical densities measured in the samples of interest and in the control, respectively.

2.2.4.3. Direct seeding of cells on porous CaP microspheres. For direct seeding of cells onto the porous CaP microspheres, immortalised Green Fluorescent Protein (GFP)-labelled human bone marrow-derived mesenchymal stem cells (hBM-MSCs) [53,54] were seeded at a density of 10×10^3 cm^{-2} [48] on 10 mg of sterile microspheres into low-adherent 48-well plates previously coated with 1% (w/v) solution of poly(2-hydroxyethyl methacrylate) (poly-HEMA, Sigma-Aldrich, UK) and Ethanol 95% in SC medium. Cells were cultured for 14 days at 37 °C and 5% CO_2. The media was refreshed every 48 h.

2.2.4.4. Presto blue assay. Metabolic activity of cells seeded on porous CaP glass microspheres was analysed using Presto Blue® (ThermoFisher Scientific, UK) reagent at day 2, day 5 and day 12 according to the manufacturer's indications. Briefly, cells were incubated with a solution of SC medium supplemented with 10% of Presto Blue at 37 °C for 40 min. The fluorescence was then measured at 560 nm and 590 nm as excitation and emission wavelengths using a plate reader Infinite 200 (Tecan, CH).

2.2.4.5. Cell staining and imaging. Cell imaging was performed at day 14 in paraformaldehyde-fixed cells. For Environmental Scanning Electron Microscopy (ESEM), post fixed cells were washed twice with distilled water and analysed using a FEI Quanta 650 ESEM microscope.

For confocal laser scanning microscopy analysis, cell nuclei were counterstained with 10 μg ml^{-1} of Hoechst 33258 for 10 min and cytoskeletal actin fibres were visualised using Vectashield mounting medium containing TRITC-Phalloidin (Vector Laboratories, UK). Confocal laser scanning microscopy was carried out on a Zeiss LSM 880 microscope using a a 10× 0.3NA or 20× 0.5NA objectives setting 5.77 μm and 1.77 μm spacing respectively and sequential imaging channels for each fluorophore. The following lasers were assigned to each fluorophore: Hoechst: $\lambda_{ex.}$ 405 nm laser, $\lambda_{em.}$ 405–437 nm, FITC-GFP: $\lambda_{ex.}$ 488 nm laser, $\lambda_{em.}$ 496–556 nm, TRITC-Phalloidin: $\lambda_{ex.}$ 561 nm laser, $\lambda_{em.}$ 564–600 nm.

2.2.5. Statistical analysis

For the cell study, one biological replicate was included in each assay. Data are presented as mean ± SEM. Statistical analysis was performed using PRISM 7.01 (GraphPad Software, USA) via the One-way ANOVA with Tukey's multiple comparison post hoc test. A 95% confidence level was considered significant.

3. Results

3.1. Surface and porous morphology of the microspheres

Both solid (non-porous) and highly porous CaP glass microspheres were produced via the flame spheroidisation process as shown in Fig. 1. Fig. 1a shows uniform non-porous glass microspheres with an average diameter of 108 (±10) μm. Fig. 1b represents the yield and distribution of pore morphologies achieved utilising the novel manufacturing process developed herein. Fig. 1c shows a SEM image of a porous CaP glass microsphere with a wide distribution of smaller surface pores (ranging from macroporous sized features to 30 μm). Whilst Fig. 1d and e highlights

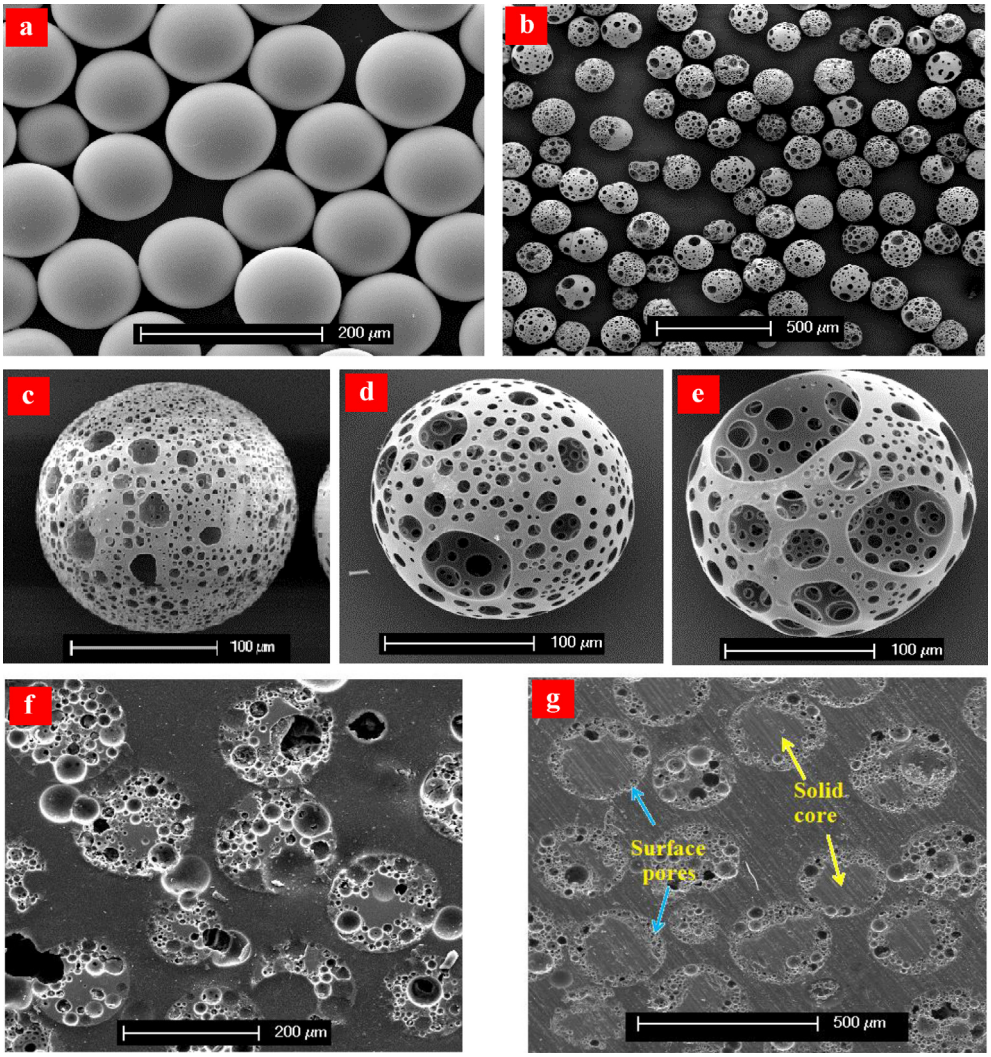

Fig. 1. Representative SEM images of solid (non-porous) and porous CaP glass microspheres: a) Shows the distribution and yield of solid microspheres, b) Scale-up production of porous glass microspheres, c) Surface morphology of porous glass microsphere with smaller surface pores, d) Porous glass microsphere with a mixture of small and large surface pores, e) Porous glass microsphere with comparatively larger surface pores, f) Cross-sectional SEM images of resin embedded porous CaP glass microspheres with interconnected open porosity, and g) Microspheres with surface pores (indicated with blue arrows) and solid core (indicated by yellow arrows). (For interpretation of the references to colour in this figure legend, the reader is referred to the web version of this article.)

porous CaP glass microspheres with a combination of larger (between 50 and 80 μm) and smaller (from 5 to 20 μm) surface pores calculated using Image J 1.51 h software (Wayne Rasband, National Institutes of Health, USA). Comparatively larger surface pores with similar internal larger interconnected pores were also produced (as shown in Fig. 1e).

The cross-sectional SEM images of the porous microspheres (as shown in Fig. 1f) revealed the inner porosity and interconnectivity of the pores, which showed that the microspheres consisted mainly of smaller pores embedded within larger pores. Microspheres with surface porosity and a solid core were also manufactured as can be seen in Fig. 1g when altering the manufacturing parameters i.e. size of initial particles.

3.2. Porosity and surface area analysis

Characterisation of the CaP microspheres revealed porosity levels of up to and over 76 (±5)% could be achieved depending on the process parameters (such as the size of the glass feed, glass powder to porogen ratio and the oxy-acetylene flame ratio utilised). Mercury porosimetry analysis of porous and solid CaP glass microspheres is shown in Fig. 2a. The mean pore size distribution for the porous microspheres was determined to be approximately 55 (±8) μm and also revealed inner pore features at the submicron and nano porosity levels (as seen in Fig. 2b). Fig. 2c highlights the percentage porosity change with increasing glass powder/porogen ratio content. The porosity of the compact solid microspheres (with a size range of between 100 and 125 μm) was found to be approximately 37 (±4)% where the interparticulate gaps between the solid microspheres were characterised as pores. However, for the porous glass microspheres porosity levels were found to be increased from 52 (±5) to 76 (±5)% by changing the glass particles to porogen ratios from 1:1 to 1:3. The surface area (ascertained via BET analysis) for the non-porous CaP microspheres was 0.09 (±0.01) $m^2 g^{-1}$ and the porous CaP microspheres were found to have an order of magnitude higher surface area which ranged from between 0.34 (±0.02) to 0.90 (±0.03) $m^2 g^{-1}$ dependant on the microsphere size range selected (see Fig. 2d). For example, the lower diameter size range porous microspheres (i.e between 63 and 125 μm) revealed a significant number of larger surface pores (hence a lower surface area of 0.34 $m^2 g^{-1}$). Whilst, a comparatively higher surface area (0.9 $m^2 g^{-1}$) was obtained for the larger diameter size range porous

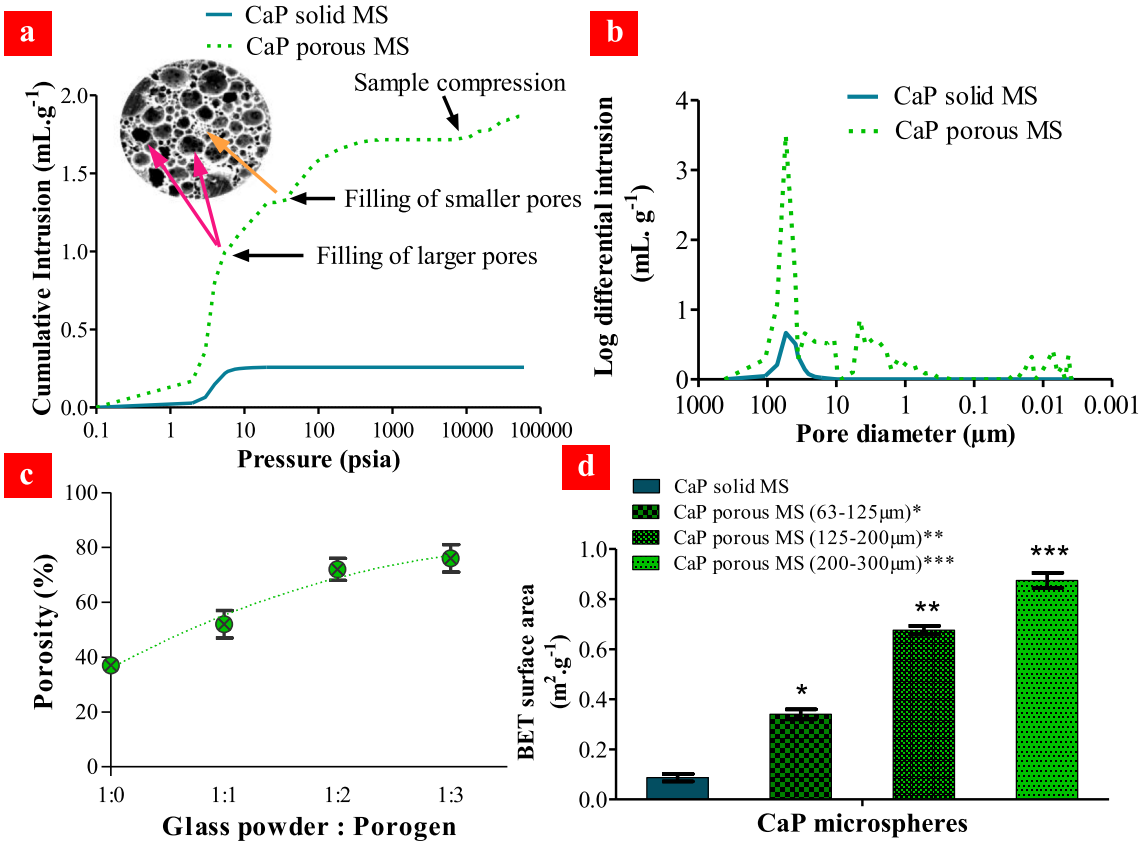

Fig. 2. Porosity and surface area properties of CaP glass microspheres: a) Mercury intrusion curves of the solid and porous CaP glass microspheres, b) log differential intrusion curves of solid and porous CaP glass microspheres highlighting the range of pore sizes achieved, c) Porosity (%) of microspheres obtained with increasing glass powder/porogen ratio content and d) BET surface area analysis of the solid and porous CaP glass microspheres (between 63 and 300 µm diameter ranges).

microspheres (i.e. between 200 and 300 µm) which revealed a larger number of smaller surface pores.

3.3. Chemical composition, degradation and ion release profiles

EDX analysis confirmed slight changes in glass compositions before and after spheroidisation (see Fig. 3a), with only localised increases in Ca content which were mainly observed around the pores created.

Porous CaP microspheres revealed an approximate 30% mass loss compared to 9% mass loss for the solid non-porous microspheres over a 28 day degradation period in ultra-purified water at 37 °C (see Fig. 3b). Fig. 3c–f show increased ion release profiles (for example, Ca^{2+} ~47 (±3) ppm, PO_4^{3-} ~49 (±3) ppm, and Mg^{2+} ~20 (±3) ppm per day) for the porous CaP glass microspheres (size range 125–200 µm) compared to the solid non-porous microspheres (Ca^{2+} ~45 (±1) ppm, PO_4^{3-} ~34 (±2) ppm, and Mg^{2+} ~13 (±1) ppm per day) when degraded in standard cell culture medium (DMEM) at 37 °C for 14 days, which was attributed to their higher surface area.

3.4. Cytocompatibility and cell viability studies

The cytocompatibility evaluation of the porous CaP glass microspheres was performed through MTT test according to the ISO standard 10993-5. Results revealed that the proliferation rate of hBM-MSCs cultured with the material ion extracts or with 1:10 serial dilutions was higher than 70% of the SC medium control (1×: 81% ± 21; 1/10×: 72% ± 16; 1/100×: 103% ± 19; 1/1000×: 87% ± 26), as showed in Fig. 4a. The suitability of the microspheres to support cell adhesion and growth was also evaluated by culturing cells directly onto the CaP glass microspheres for up to 14 days in SC medium. Their metabolic activity was analysed at 12 h, day 5 and day 12 which showed a progressive increase of the signal over time, suggesting an increase in cell numbers (see Fig. 4b).

Initial observations confirmed through ESEM imaging showed that the cells were indeed attached and had spread on the microspheres and could also be observed in their inner pore structures (*indicated by yellow arrows*) (Fig. 5a, b).

Further detailed analysis using scanning laser confocal microscopy was performed at day 14, where it was clearly observed that cells were attached to the microspheres and grew on and around them forming macro-aggregates (Fig. 5c, d). Moreover, fluorescent cells were detected in the inner side of the microspheres at different levels through the z-stack, suggesting their localisation within the pores (indicated by white arrows, Fig. 5e).

4. Discussion

Orthobiologic therapies are being developed to help improve the long-term health of patients suffering from disabling musculoskeletal disorders and is a rapidly advancing field which utilises cell-based therapies and biomaterials to promote healing and offers exciting alternatives to traditional orthopaedic options.

The results above demonstrate (for the first time, to the best of the authors' knowledge) a successful production process to manufacture porous CaP glass microspheres. The manufacturing route developed relies on a number of key parameters including the chemical and physical interaction of the porogen with the glass

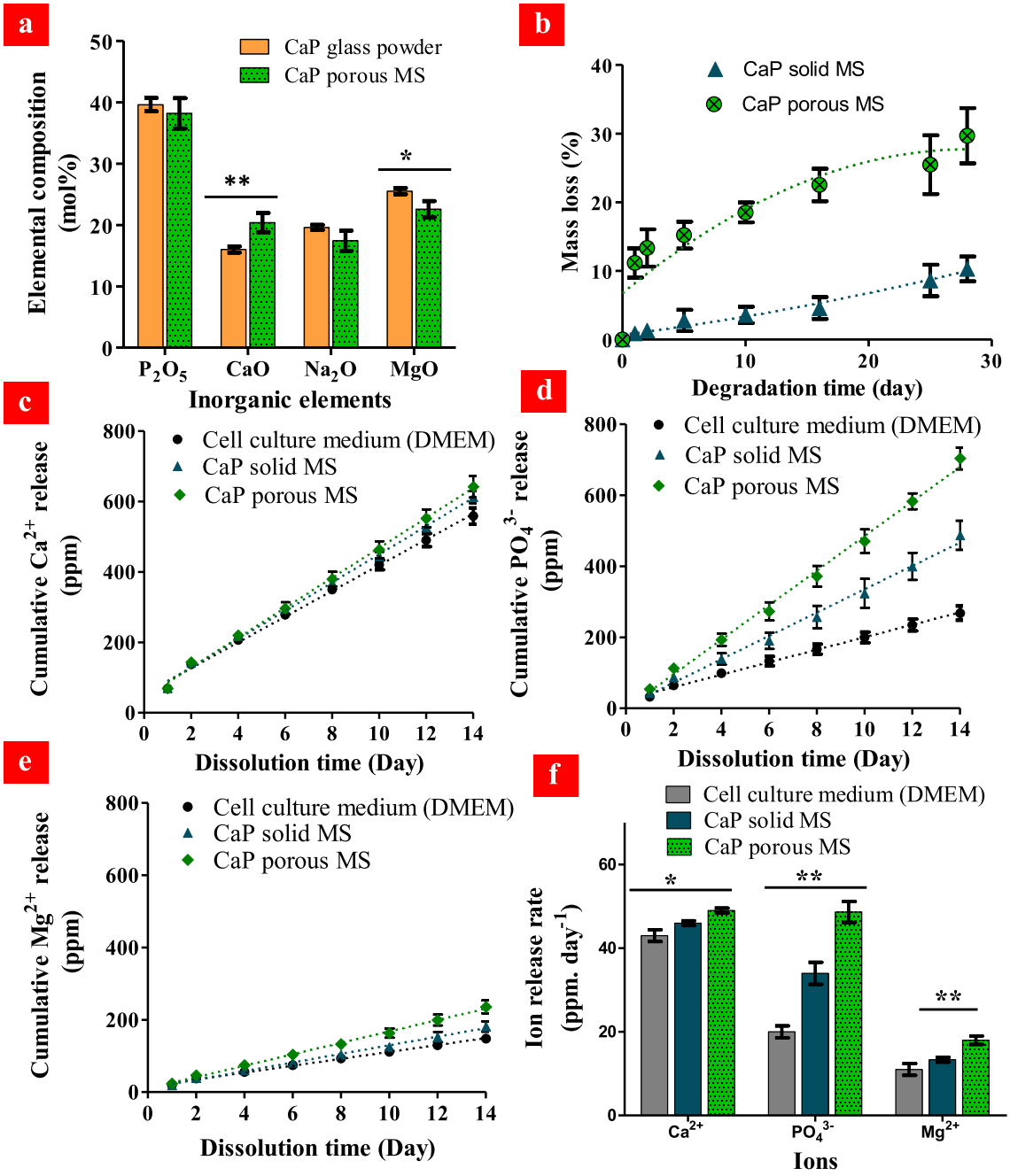

Fig. 3. Chemical composition, degradation and ion release profiles of CaP glass microspheres: a) Chemical composition of the glass (ascertained via EDX analysis) before and after spheroidisation, b) Mass loss profiles of solid and porous CaP glass microspheres during degradation in ultra purified over 28 days at 37 °C, and c–e) Cumulative ion release profile (Ca^{2+}, PO_4^{3-}, and Mg^{2+}) of solid and porous CaP microspheres in DMEM cell culture medium over 14 days at 37 °C, and f) ion release rates (ppm per day) of solid and porous CaP microspheres calculated from the linear cumulative ion release profiles (observed in c–e). ($^{*}p < 0.05$, $^{**}p < 0.01$).

the glass viscosity, along with both being delivered within a suitable thermal processing window.

Fig. 6 highlights a schematic representation of the morphological changes that occur and the proposed underlying mechanisms to produce the porous glass microspheres. The manufacturing process involved selection of a glass formulation that will not only melt but then allows it to reach a temperature where the viscosity was sufficiently low such that entrapment of the porogen gas could occur within the molten particle, which was itself driven to produce a spherical morphology due to surface tension from being ejected from the flame. The kinetics of decomposition must ideally be sufficiently slow for gas entrapment and adequately fast for pore formation to occur.

Critical to this process was not only the choice of the pore-forming agent but also the size of the porogens and in some cases how they were applied to affect the pore sizes and levels produced. As shown in Fig. 1, a range of pores, pore sizes and quantities are achievable from this process. Furthermore, it was also found that varying the initial particle size and porogen quantities, enabled control over the size of the surface and interconnected pores.

Examining the CaP porous glass microspheres reported here the porosity (as measured via mercury intrusion) showed an increase

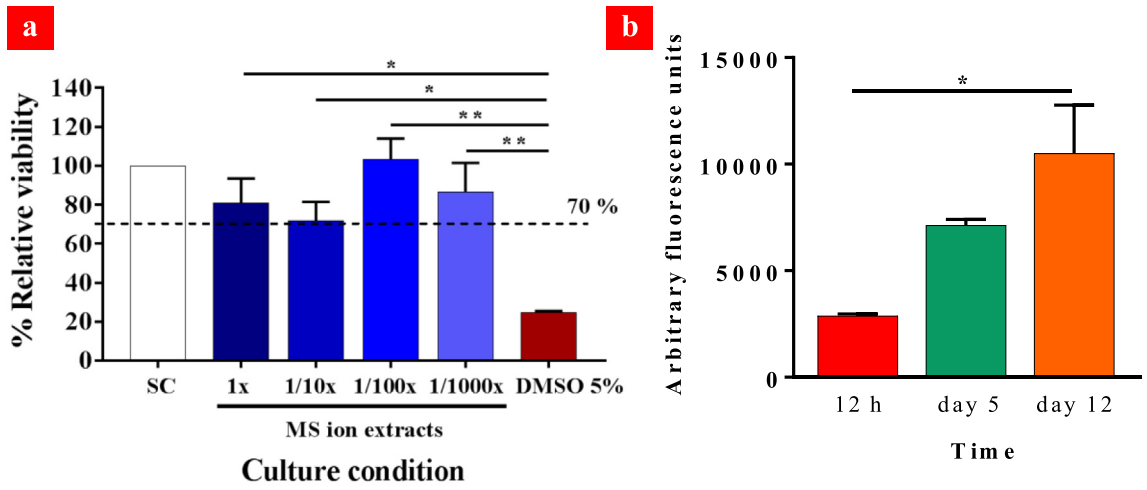

Fig. 4. Cytocompatibility evaluation of porous CaP glass microspheres. a) Results of MTT test showing the relative viability of cells cultured with ion extract conditioned medium (1×) and for the following three serial dilutions (1/10×, 1/100×, 1/1000×). The SC medium only and SC supplemented with 5% DMSO were included as a control. b) Shows the results of cell metabolic activity of hBM-MSCs cultured on the porous CaP microspheres for 12 h, 5 and 12 days for porous CaP microspheres cultured at 12 h, day 5 and day 12 after seeding ($^{*}p < 0.05$, $^{**}p < 0.01$).

from approximately 37% for loosely packed non-porous microspheres, which is typical for packed spheres, to over 76% for the porous microspheres (see Fig. 2a–c). These results revealed that the inter-particulate gaps also contributed to the overall porosity levels measured for both the solid (non-porous) and the porous microspheres.

This study also showed that both porogen quantity and microparticles size also effected pore size and surface area, as higher quantities of porogen resulted in increased porosity (see Fig. 2c) and smaller (63–125 μm) particle sizes resulted in larger pore sizes. BET analysis confirmed that surface area could also be controlled up to approximately 0.9 $m^2 g^{-1}$ (see Fig. 2d). These values appeared to be low, however the resulting porous microspheres resemble a shell-like structure with fully interconnected pores, which was reflected in the values obtained.

Addition of porogen during the spheroidisation process also resulted in slightly localised increase in Ca content which was mainly observed around the pores (see Fig. 3a) and was attributed to the use of Ca-based porogen utilised. The introduction of porosity also resulted in an increase in mass loss during degradation (see Fig. 3b) and increased the release of ions as expected due to the increased surface area achieved. As such, by simple selection of glass formulations and particle size, the microsphere porosity levels (which in turn relates to their surface area) could easily be manipulated to control ion release rates (as seen in Fig. 3c–e) of potentially biotherapeutic ions for specific end applications.

The advantages of larger surface pores are that they could be exploited for applications which require faster ingress of fluids or media through the internal microsphere structure and smaller pores within could be utilised for the entrapment of particulate materials, for example in separation sciences. In particular for biomedical applications, larger pores would be beneficial to accommodate particular cell types, in order to promote tissue engineering or regeneration activities, whereas smaller surface pores could be beneficial for controlling the release of drugs and/or other small biological components or biomolecules, entrapped within. Furthermore, where biological cell and material interactions are concerned, the inter-particulate gaps between the microspheres along with the enhanced levels of interconnected porosity created using this simple, single stage manufacturing process, could enable permeation of nutrients and waste products throughout the entire cell/material constructs [55,56].

Recently it has been shown that cell fate, in particular, stem cell phenotype, could be influenced by controlled release of specific ions from inorganic materials [58]. Through simple compositional tailoring, the formulation of CaP glasses can easily be modified to release ions of specific interest. The solid and porous microspheres manufactured in this study revealed release of Ca^{2+}, PO_4^{3-} and Mg^{2+} ions ranging from 45 to 47, 34–49 and 13–20 ppm per day (see Fig. 3f). Furthermore, studies by Ahmed et al. [59], showed that phosphate anionic species (ranging from ortho, pyro, meta and polyphosphates) could also be controlled, by simple tailoring of the starting glass formulations.

Fig. 7 highlights some of the ions which could be released from CaP glasses and their potential biotherapeutic roles in bone repair and regeneration. Ca^{2+} ions are known to stimulate proliferation and differentiation of osteoblasts as well as extracellular matrix mineralisation [60] whilst Mg^{2+} ions can promote new bone formation [61]. Moreover, PO_4^{3-} ions are required for calcium phosphate crystal deposition [62] and extracellular matrix mineralisation while Na^{+} ions are mainly found in extracellular fluid [63].

Other biotherapeutic ions can also be released from the CaP microspheres such as Sr^{2+} [13], Cu^{2+} [10] and Ag^{+} [11] by simply doping the glass composition with the desired metal oxide. For instance, Sr^{2+} ions are known to inhibit osteoclast activity whilst promoting osteogenesis of mesenchymal stem cells *in vitro* and *in vivo* [64–66], Ag^{2+} and Cu^{2+} ions have both demonstrated antimicrobial properties [10,67] while Cu^{2+} ions have been also been shown to increase vascular endothelial growth factor (VEGF) expression [68], which are associated with the angiogenesis process [69].

This study also demonstrated that the porous microspheres produced were biocompatible (see Fig. 4a) according to the standard ISO 10993-5 (i.e. used for the biological evaluation of biomedical devices). Moreover, when the cells were seeded and cultured directly onto the microspheres, they were not only able to attach but had also migrated to within the centre of the microspheres, revealing colonisation of the inner pore structures (see Fig. 5e). The pores formed presented the cells with a high surface area and a niche environment for the cells to grow and proliferate, acting as sites for cell culture [70]. This niche pore environment could also reduce any potential shear stresses experienced by the cells and provide protection for cells from getting damaged via inter-particle abrasion. Furthermore, the pores also closely resemble

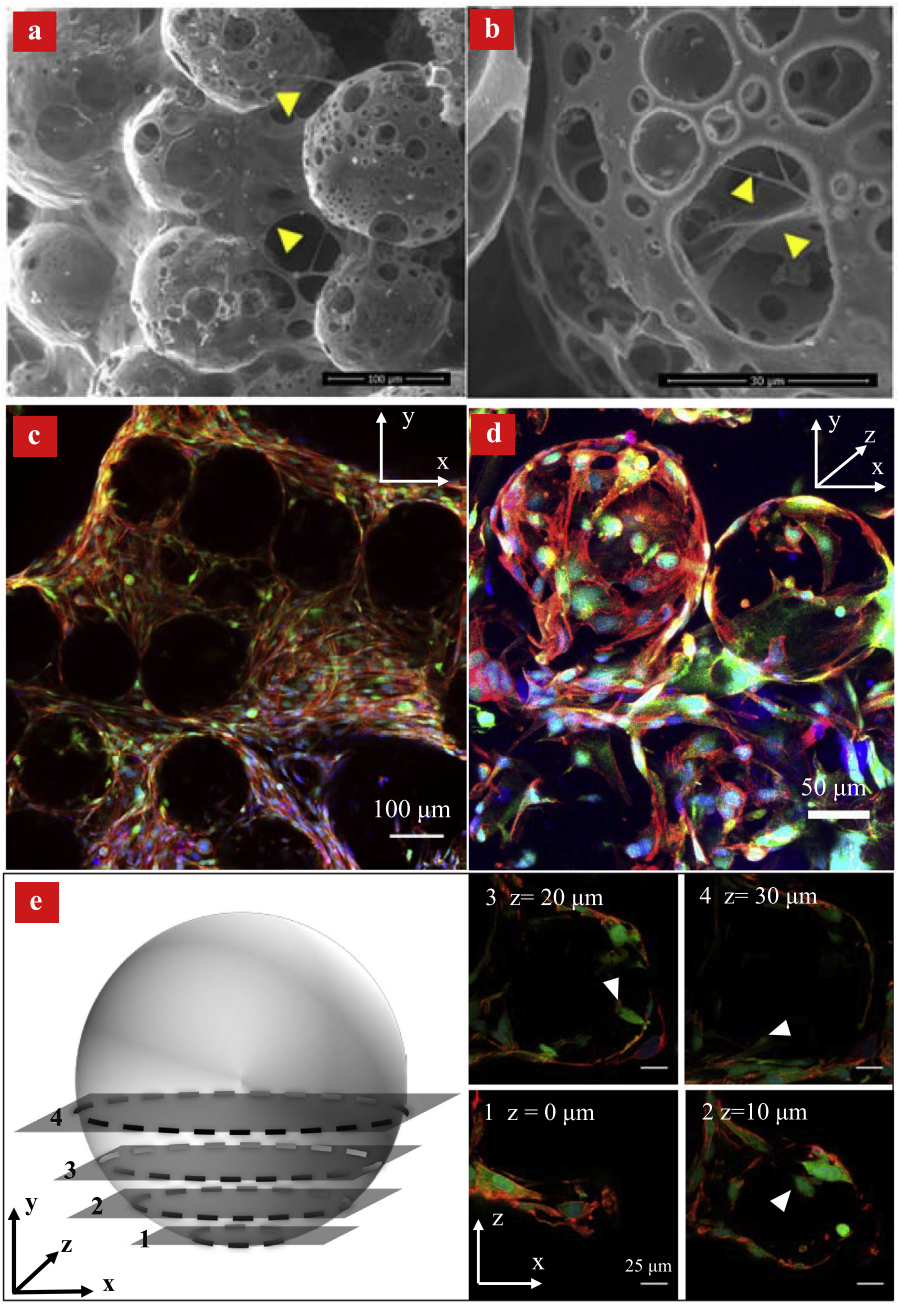

Fig. 5. a) ESEM image of stem cell-microsphere aggregates; the yellow arrows indicate hBM-MSCs attached and bridging across several microspheres, b) ESEM image shows colonisation of hBM-MSCs within the pores of the microspheres (yellow arrows), c, d) Representative confocal images (in single plane and z-stacked mode) of GFP-labelled hBM-MSCs seeded on porous CaP microspheres at day 14, and e) cross-sectioned representation of a microsphere and its respective single plane sectioned images; white arrows indicate cells which have migrated internally within the microsphere. hBM-MSCs are seen in green (GFP), the nuclei are stained in blue (Hoechst 33259) and the cytoskeleton is seen in red (Phalloidin), respectively. Scale bars: 100 µm (c), 50 µm (d) and 25 µm (e). (For interpretation of the references to colour in this figure legend, the reader is referred to the web version of this article.)

the native 3D conformation of bone tissue [71]. It has also been proposed that a porous environment would favour the capture and utilisation of cell secreted factors close to where the cells reside in order to further influence cell phenotype [58].

The porous microspheres developed in this study constitute a versatile and highly promising technology for wider applications in tissue engineering and regenerative medicine (with a particular focus in bone regeneration) as initial examples. Indeed, doping the starting glass formulations with specific biotherapeutic ions could also address other key aspects of bone regeneration to include angiogenesis, osteogenesis and control of osteoclast activity, all potentially also coupled with antimicrobial properties. Further studies are on-going aimed at investigating more in-depth the bone tissue regenerative potential of these microspheres as well as exploring their potential use in alternate biomedical applications.

The porous glass microsphere production process developed herein offers a new cost-effective single stage manufacturing process, with demonstrated scale-up potential and with production levels in the range of kg's per hour at lab scale, which could easily be further scaled-out to commercial scales. Follow-on investigations are on-going to explore the utility of this manufacturing

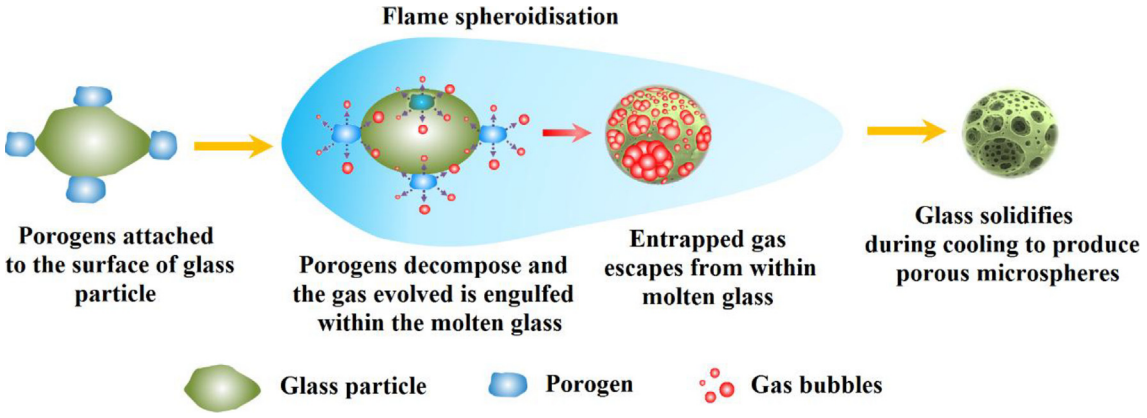

Fig. 6. Schematic representation of the proposed mechanism for manufacturing porous glass microspheres via the flame spheroidisation process. The decomposition temperature of the porogen is key in matching the melt temperature profile of the glass.

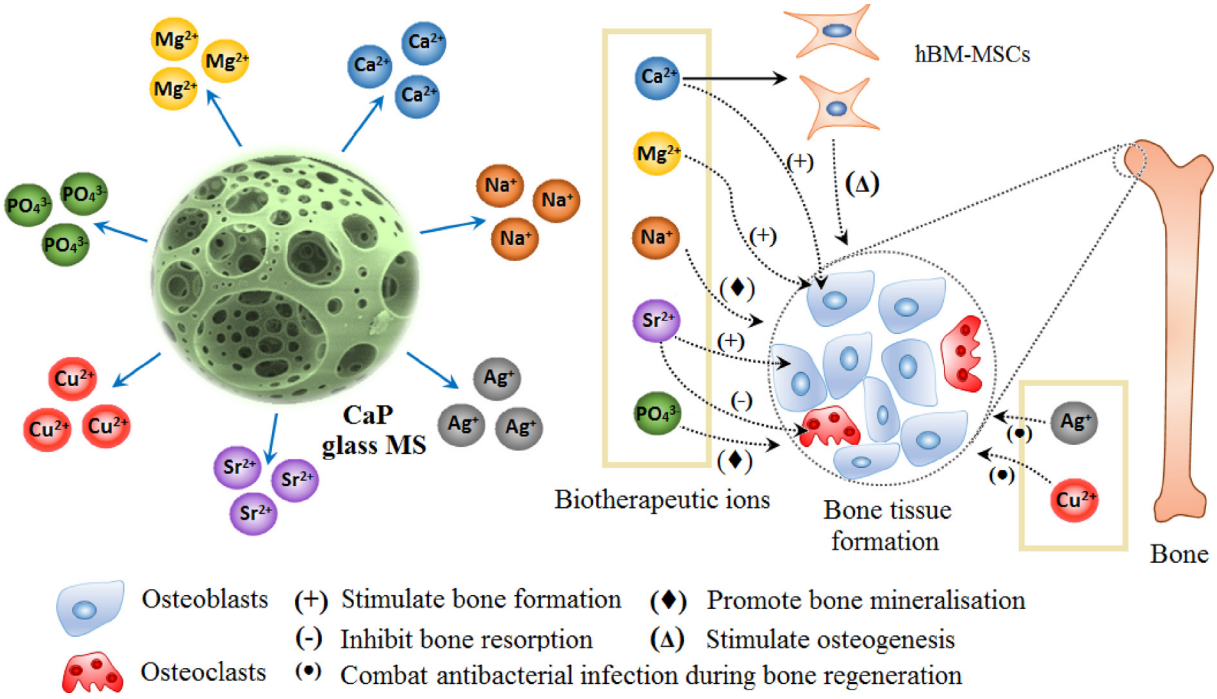

Fig. 7. Biotherapeutic ions which can be released from CaP glass and their role in bone tissue formation.

process for other glass types (i.e. borates and silicates including glass-ceramics).

5. Conclusions

This study highlights a novel flame spheroidisation process to manufacture highly porous CaP glass microspheres. Microspheres with a range of surface and fully interconnected porosity from 52 (±5) to 76 (±5)% were manufactured by simply manipulating process parameters such as the ratios of glass particles to porogen used (from 1:1 to 1:3) including the oxy-acetylene gas ratios. The manufacturing process involved selection of glass formulations and porogens (which matched the melting temperature of the glass formulation with the decomposition profile of the porogen).

Addition of porogen during the spheroidisation process also resulted in a localised increase in Ca content which was observed around the pores due to the use of Ca-based porogen. The increase in porosity levels of the microspheres was shown to accelerate degradation over a 28 day degradation period (i.e. a 30% mass loss was observed for porous microspheres, compared to a 9% mass loss for the solid non-porous microspheres). The ion release profiles of the porous microspheres also revealed increasing rates as expected, compared to the non-porous microspheres, which was attributed to their increased surface area profiles.

The cell culture study revealed that the ion extracts from the CaP microspheres (utilising indirect cell culture method according to ISO 10993) did not exert any negative effect on the stem cells (hBM-MSCs). In addition, the direct cell culture study revealed that the porous microspheres supported cell attachment as well as proliferation and showed that the hBM-MSCs had migrated into and towards the centre of the microspheres. The pore sizes and porosity levels achieved opens up the potential for use of these porous

CaP microspheres for other biomedical applications in addition to the proposed orthobiologic applications.

Acknowledgements

This work has been funded through the RDF-PP-0303 (University of Nottingham), IKC University of Leeds (EP/G032483/1), EPSRC IAA (University of Nottingham, ref. no. EP/K503800/1), Science and Technology Facilities Council (ST/L502583/1) and the National Institute for Health Research (NIHR) Invention for Innovation (i4i) Challenge Award Programme (II-C3-0714-20001). The views expressed above are those of the authors and not necessarily those of the NHS, the NIHR or the Department of Health.

The authors would also like to acknowledge Nicola Weston at the Nanoscale and Microscale Research Centre (NMRC) at the University of Nottingham for use of the electron microscope facilities and Dr Christhopher Gell of the University of Nottingham's School of Life Sciences Imaging (SLIM) for the use of confocal microscopy and help with image analysis.

Appendix A. Supplementary data

Supplementary data associated with this article can be found, in the online version, at https://doi.org/10.1016/j.actbio.2018.03.040.

References

[1] A. Weglein, S. Sampson, D. Aufiero, Platelet rich plasma practical use in non-surgical musculoskeletal pathology, in: J.F.S.D. Lana, M.H. Andrade Santana, W. Dias Belangero, A.C. Malheiros Luzo (Eds.), Platelet-Rich Plasma: Regenerative Medicine: Sports Medicine, Orthopedic, and Recovery of Musculoskeletal Injuries, Springer Berlin Heidelberg, Berlin, Heidelberg, 2014, pp. 187–201.
[2] S. Sampson, A.B.-V. Bemden, D. Aufiero, Autologous bone marrow concentrate: review and application of a novel intra-articular orthobiologic for cartilage disease, Phys. Sports Med. 41 (3) (2013) 7–18.
[3] B.C. Toolan, Current concepts review: orthobiologics, Foot Ankle Int. 27 (7) (2006) 561–566.
[4] Z. Sheikh, N. Hamdan, Y. Ikeda, M. Grynpas, B. Ganss, M. Glogauer, Natural graft tissues and synthetic biomaterials for periodontal and alveolar bone reconstructive applications: a review, Biomater. Res. 21 (2017) 9.
[5] L.L. Hench, J.R. Jones, Bioactive glasses: frontiers and challenges, Front. Bioeng. Biotechnol. 3 (194) (2015).
[6] L.L. Hench, The story of Bioglass®, J. Mater. Sci. Mater. Med. 17 (11) (2006) 967–978.
[7] X. Zhang, D. Zeng, N. Li, J. Wen, X. Jiang, C. Liu, Y. Li, Functionalized mesoporous bioactive glass scaffolds for enhanced bone tissue regeneration, Sci. Rep. 6 (2016) 19361.
[8] J.R. Jones, L.M. Ehrenfried, L.L. Hench, Optimising bioactive glass scaffolds for bone tissue engineering, Biomaterials 27 (7) (2006) 964–973.
[9] W. Huang, D.E. Day, K. Kittiratanapiboon, M.N. Rahaman, Kinetics and mechanisms of the conversion of silicate (45S5), borate, and borosilicate glasses to hydroxyapatite in dilute phosphate solutions, J. Mater. Sci. Mater. Med. 17 (7) (2006) 583–596.
[10] E.A. Abou Neel, I. Ahmed, J. Pratten, S.N. Nazhat, J.C. Knowles, Characterisation of antibacterial copper releasing degradable phosphate glass fibres, Biomaterials 26 (15) (2005) 2247–2254.
[11] I. Ahmed, E.A. Abou Neel, S.P. Valappil, S.N. Nazhat, D.M. Pickup, D. Carta, D.L. Carroll, R.J. Newport, M.E. Smith, J.C. Knowles, The structure and properties of silver-doped phosphate-based glasses, J. Mater. Sci. 42 (23) (2007) 9827–9835.
[12] E.A. Abou Neel, W. Chrzanowski, J.C. Knowles, Effect of increasing titanium dioxide content on bulk and surface properties of phosphate-based glasses, Acta Biomater. 4 (3) (2008) 523–534.
[13] U. Patel, R.M. Moss, K.M.Z. Hossain, A.R. Kennedy, E.R. Barney, I. Ahmed, A.C. Hannon, Structural and physico-chemical analysis of calcium/strontium substituted, near-invert phosphate based glasses for biomedical applications, Acta Biomater. 60 (Suppl. C) (2017) 109–127.
[14] I. Ahmed, A. Parsons, A. Jones, G. Walker, C. Scotchford, C. Rudd, Cytocompatibility and effect of Increasing MgO content in a range of quaternary invert phosphate-based glasses, J. Biomater. Appl. 24 (6) (2010) 555–575.
[15] E.A. Abou Neel, L.A. O'Dell, W. Chrzanowski, M.E. Smith, J.C. Knowles, Control of surface free energy in titanium doped phosphate based glasses by co-doping with zinc, J. Biomed. Mater. Res. B: Appl. Biomater. 89 (2) (2009 May) 392–407.
[16] M. Bitar, V. Salih, J.C. Knowles, M.P. Lewis, Iron-phosphate glass fiber scaffolds for the hard-soft interface regeneration: the effect of fiber diameter and flow culture condition on cell survival and differentiation, J. Biomed. Mater. Res. A 87 (4) (2008 Dec 15) 1017–1026.
[17] N.J. Lakhkar, E.A. Abou Neel, V. Salih, J.C. Knowles, Strontium oxide doped quaternary glasses: effect on structure, degradation and cytocompatibility, J. Mater. Sci. Mater. Med. 20 (6) (2009) 1339–1346 (Epub 10.01.09).
[18] S.P. Valappil, D.M. Pickup, D.L. Carroll, C.K. Hope, J. Pratten, R.J. Newport, M.E. Smith, M. Wilson, J.C. Knowles, Effect of silver content on the structure and antibacterial activity of silver-doped phosphate-based glasses, Antimicrob. Agents Chemother. 51 (12) (2007) 4453–4461 (Epub 01.10.07).
[19] S.P. Valappil, D. Ready, E.A. Abou Neel, D.M. Pickup, L.A. O'Dell, W. Chrzanowski, J. Pratten, R.J. Newport, M.E. Smith, M. Wilson, J.C. Knowles, Controlled delivery of antimicrobial gallium ions from phosphate-based glasses, Acta Biomater. 5 (4) (2009) 1198–1210 (Epub 10.10.08).
[20] I. Ahmed, M. Lewis, I. Olsen, J.C. Knowles, Phosphate glasses for tissue engineering: Part 2. Processing and characterisation of a ternary-based P2O5-CaO-Na2O glass fibre system, Biomaterials 25 (3) (2004) 501–507.
[21] I. Ahmed, M. Lewis, I. Olsen, J.C. Knowles, Phosphate glasses for tissue engineering: Part 1. Processing and characterisation of a ternary-based P2O5–CaO–Na2O glass system, Biomaterials 25 (3) (2004) 491–499.
[22] S. Freiberg, X.X. Zhu, Polymer microspheres for controlled drug release, Int. J. Pharm. 282 (1–2) (2004) 1–18.
[23] N.J. Lakhkar, J.-H. Park, N.J. Mordan, V. Salih, I.B. Wall, H.-W. Kim, S.P. King, J.V. Hanna, R.A. Martin, O. Addison, J.F.W. Mosselmans, J.C. Knowles, Titanium phosphate glass microspheres for bone tissue engineering, Acta Biomater. 8 (11) (2012) 4181–4190.
[24] M. Bohner, S. Tadier, N. van Garderen, A. de Gasparo, N. Döbelin, G. Baroud, Synthesis of spherical calcium phosphate particles for dental and orthopedic applications, Biomatter 3 (2) (2013) e25103.
[25] S. Mitragotri, P.A. Burke, R. Langer, Overcoming the challenges in administering biopharmaceuticals: formulation and delivery strategies, Nat. Rev. Drug Discov. 13 (9) (2014) 655–672.
[26] Y. Cai, Y. Chen, X. Hong, Z. Liu, W. Yuan, Porous microsphere and its applications, Int. J. Nanomed. 8 (2013) 1111–1120.
[27] S. Li, L. Nguyen, H. Xiong, M. Wang, T.C.C. Hu, J.-X. She, S.M. Serkiz, G.G. Wicks, W.S. Dynan, Porous-wall hollow glass microspheres as novel potential nanocarriers for biomedical applications, Nanomed. Nanotechnol. Biol. Med. 6 (1) (2010) 127–136.
[28] V.V. Budov, Hollow glass microspheres: use, properties, and technology (review), Glass Ceram. 51 (7–8) (1994) 230–235.
[29] S. Labbaf, O. Tsigkou, K.H. Müller, M.M. Stevens, A.E. Porter, J.R. Jones, Spherical bioactive glass particles and their interaction with human mesenchymal stem cells in vitro, Biomaterials 32 (4) (2011) 1010–1018.
[30] X. Zhao, S. Liu, L. Yildirimer, H. Zhao, R. Ding, H. Wang, W. Cui, D. Weitz, Injectable stem cell-laden photocrosslinkable microspheres fabricated using microfluidics for rapid generation of osteogenic tissue constructs, Adv. Funct. Mater. 26 (17) (2016) 2809–2819.
[31] K.J. Pekarek, J.S. Jacob, E. Mathiowitz, Double-walled polymer microspheres for controlled drug release, Nature 367 (6460) (1994) 258–260.
[32] X. Liu, X. Jin, P.X. Ma, Nanofibrous hollow microspheres self-assembled from star-shaped polymers as injectable cell carriers for knee repair, Nat. Mater. 10 (5) (2011) 398–406.
[33] W. Li, J.Y. Walz, Porous nanocomposites with integrated internal domains: application to separation membranes, Sci. Rep. 4 (2014).
[34] Z.-C. Yang, C.-H. Tang, Y. Zhang, H. Gong, X. Li, J. Wang, Cobalt monoxide-doped porous graphitic carbon microspheres for supercapacitor application, Sci. Rep. 3 (2013).
[35] Y.N. Ko, S.B. Park, S.H. Choi, Y.C. Kang, One-pot synthesis of manganese oxide-carbon composite microspheres with three dimensional channels for Li-ion batteries, Sci. Rep. 4 (2014).
[36] H.X. Peng, Z. Fan, J.R.G. Evans, J.J.C. Busfield, Microstructure of ceramic foams, J. Eur. Ceram. Soc. 20 (7) (2000) 807–813.
[37] L. Montanaro, Y. Jorand, G. Fantozzi, A. Negro, Ceramic foams by powder processing, J. Eur. Ceram. Soc. 18 (9) (1998) 1339–1350.
[38] D. Enke, R. Gläser, U. Tallarek, Sol-gel and porous glass-based silica monoliths with hierarchical pore structure for solid-liquid catalysis, Chemie Ingenieur Technik 88 (11) (2016) 1561–1585.
[39] Z.Y. Wu, R.G. Hill, S. Yue, D. Nightingale, P.D. Lee, J.R. Jones, Melt-derived bioactive glass scaffolds produced by a gel-cast foaming technique, Acta Biomater. 7 (4) (2011) 1807–1816.
[40] Q. Fu, E. Saiz, A.P. Tomsia, Bioinspired strong and highly porous glass scaffolds, Adv. Funct. Mater. 21 (6) (2011) 1058–1063.
[41] S. Hyuk Im, U. Jeong, Y. Xia, Polymer hollow particles with controllable holes in their surfaces, Nat. Mater. 4 (9) (2005) 671–675.
[42] S.-W. Choi, Y. Zhang, Y.-C. Yeh, A. Lake Wooten, Y. Xia, Biodegradable porous beads and their potential applications in regenerative medicine, J. Mater. Chem. 22 (23) (2012) 11442–11451.
[43] H.-H. Lee, S.-J. Hong, C.-H. Kim, E.-C. Kim, J.-H. Jang, H.-I. Shin, H.-W. Kim, Preparation of hydroxyapatite spheres with an internal cavity as a scaffold for hard tissue regeneration, J. Mater. Sci. Mater. Med. 19 (9) (2008) 3029–3034.
[44] M. Kawashita, S. Toda, H.-M. Kim, T. Kokubo, N. Masuda, Preparation of antibacterial silver-doped silica glass microspheres, J. Biomed. Mater. Res. A 66A (2) (2003) 266–274.
[45] D. Enke, F. Janowski, W. Schwieger, Porous glasses in the 21st century – a short review, Microporous Mesoporous Mater. 60 (1) (2003) 19–30.
[46] U. Patel, R.M. Moss, K.M.Z. Hossain, A.R. Kennedy, E.R. Barney, I. Ahmed, A.C. Hannon, Structural and physico-chemical analysis of calcium/strontium

substituted, near-invert phosphate based glasses for biomedical applications, Acta Biomater. 60 (2017) 109–127.
[47] M.S. Hasan, I. Ahmed, A.J. Parsons, G.S. Walker, C.A. Scotchford, Material characterisation and cytocompatibility assessment of quinternary phosphate glasses, J. Mater. Sci. Mater. Med. 23 (10) (2012) 2531–2541.
[48] G. Dhanak, M.G. David, M.Z.H. Kazi, A. Ifty, S. Virginie, Role of geometrical cues in bone marrow-derived mesenchymal stem cell survival, growth and osteogenic differentiation, J. Biomater. Appl. 32 (7) (2017) 906–919.
[49] H. Liu, H. Yazici, C. Ergun, T.J. Webster, H. Bermek, An in vitro evaluation of the Ca/P ratio for the cytocompatibility of nano-to-micron particulate calcium phosphates for bone regeneration, Acta Biomater. 4 (5) (2008) 1472–1479.
[50] L.A. France, C.A. Scotchford, D.M. Grant, H. Rashidi, A.A. Popov, V. Sottile, Transient serum exposure regimes to support dual differentiation of human mesenchymal stem cells, J. Tissue Eng. Regener. Med. 8 (8) (2014) 652–663.
[51] T. Okamoto, T. Aoyama, T. Nakayama, T. Nakamata, T. Hosaka, K. Nishijo, T. Nakamura, T. Kiyono, J. Toguchida, Clonal heterogeneity in differentiation potential of immortalized human mesenchymal stem cells, Biochem. Biophys. Res. Commun. 295 (2) (2002) 354–361.
[52] H. Rashidi, S. Strohbuecker, L. Jackson, S. Kalra, A.J. Blake, L. France, C. Tufarelli, V. Sottile, Differences in the pattern and regulation of mineral deposition in human cell lines of osteogenic and non-osteogenic origin, Cells Tissues Organs 195 (6) (2012) 484–494.
[53] R. Harrison, H. Markides, R.H. Morris, P. Richards, A.J. El Haj, V. Sottile, Autonomous magnetic labelling of functional mesenchymal stem cells for improved traceability and spatial control in cell therapy applications, J. Tissue Eng. Regener. Med. 11 (8) (2017) 2333–2348.
[54] L. Macri-Pellizzeri, N. De Melo, I. Ahmed, D. Grant, B. Scammell, V. Sottile, Live quantitative monitoring of mineral deposition in stem cells using tetracycline hydrochloride, Tissue Eng. Part C: Methods (2018).
[55] Y. Senuma, S. Franceschin, J.G. Hilborn, P. Tissiéres, P. Frey, Bioresorbable microspheres as injectable cell carrier: from preparation to in vitro evaluation, MRS Proc. 550 (1998).
[56] O. Qutachi, J.R. Vetsch, D. Gill, H. Cox, D.J. Scurr, S. Hofmann, R. Müller, R.A. Quirk, K.M. Shakesheff, C.V. Rahman, Injectable and porous PLGA microspheres that form highly porous scaffolds at body temperature, Acta Biomater. 10 (12) (2014) 5090–5098.
[57] Y. Cai, Y. Chen, X. Hong, Z. Liu, W. Yuan, Porous microsphere and its applications, Int. J. Nanomed. 8 (2013) 1111–1120.
[58] W.L. Murphy, T.C. McDevitt, A.J. Engler, Materials as stem cell regulators, Nat. Mater. 13 (6) (2014) 547–557.
[59] I. Ahmed, M.P. Lewis, S.N. Nazhat, J.C. Knowles, Quantification of anion and cation release from a range of ternary phosphate-based glasses with fixed 45 mol% P_2O_5, J. Biomater. Appl. 20 (1) (2005) 65–80.
[60] S. Maeno, Y. Niki, H. Matsumoto, H. Morioka, T. Yatabe, A. Funayama, Y. Toyama, T. Taguchi, J. Tanaka, The effect of calcium ion concentration on osteoblast viability, proliferation and differentiation in monolayer and 3D culture, Biomaterials 26 (23) (2005) 4847–4855.
[61] S. Yoshizawa, A. Brown, A. Barchowsky, C. Sfeir, Role of magnesium ions on osteogenic response in bone marrow stromal cells, Connect. Tissue Res. 55 (2014) 155–159.
[62] M. Julien, S. Khoshniat, A. Lacreusette, M. Gatius, A. Bozec, E.F. Wagner, Y. Wittrant, M. Masson, P. Weiss, L. Beck, D. Magne, J. Guicheux, Phosphate-dependent regulation of MGP in osteoblasts: role of ERK1/2 and Fra-1, J. Bone Miner. Res. 24 (11) (2009) 1856–1868.
[63] D.I. Hamasaki, The effect of sodium ion concentration on the electroretinogram of the isolated retina of the frog, J. Physiol. 167 (1) (1963) 156–168.
[64] V. Mouriño, J.P. Cattalini, A.R. Boccaccini, Metallic ions as therapeutic agents in tissue engineering scaffolds: an overview of their biological applications and strategies for new developments, J. R. Soc. Interface 9 (68) (2012) 401–419.
[65] S. Kargozar, N. Lotfibakhshaiesh, J. Ai, M. Mozafari, P. Brouki Milan, S. Hamzehlou, M. Barati, F. Baino, R.G. Hill, M.T. Joghataei, Strontium- and cobalt-substituted bioactive glasses seeded with human umbilical cord perivascular cells to promote bone regeneration via enhanced osteogenic and angiogenic activities, Acta Biomater. 58 (2017) 502–514.
[66] L. Weng, S.K. Boda, M.J. Teusink, F.D. Shuler, X. Li, J. Xie, Binary doping of strontium and copper enhancing osteogenesis and angiogenesis of bioactive glass nanofibers while suppressing osteoclast activity, ACS Appl. Mater. Interfaces 9 (29) (2017) 24484–24496.
[67] I. Ahmed, D. Ready, M. Wilson, J.C. Knowles, Antimicrobial effect of silver-doped phosphate-based glasses, J. Biomed. Mater. Res. Part A 79A (3) (2006) 618–626.
[68] S.N. Rath, A. Brandl, D. Hiller, A. Hoppe, U. Gbureck, R.E. Horch, A.R. Boccaccini, U. Kneser, Bioactive copper-doped glass scaffolds can stimulate endothelial cells in co-culture in combination with mesenchymal stem cells, PLoS ONE 9 (12) (2014) 1–24.
[69] C. Gérard, L.-J. Bordeleau, J. Barralet, C.J. Doillon, The stimulation of angiogenesis and collagen deposition by copper, Biomaterials 31 (5) (2010) 824–831.
[70] D. Looby, B. Griffiths, Immobilization of animal cells in porous carrier culture, Trends Biotechnol. 8 (1990) 204–209.
[71] L. Andrea Di, L. Alessia, C. Giuseppe, M. Carlos, B. Clemens, M. Lorenzo, Toward mimicking the bone structure: design of novel hierarchical scaffolds with a tailored radial porosity gradient, Biofabrication 8 (4) (2016) 045007.